

Light-Induced Non-Thermal Phase Transition To The Topological Crystalline Insulator State In SnSe

Stefano Mocatti,* Giovanni Marini,* and Matteo Calandra*

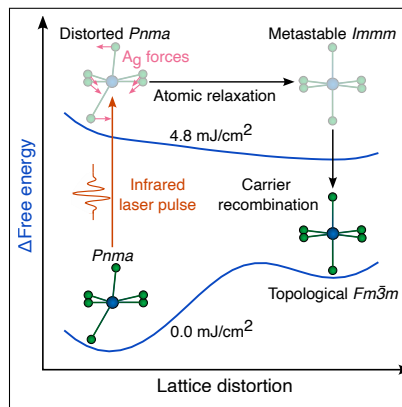
Department of Physics, University of Trento, Via Sommarive 14, 38123 Povo, Italy

E-mail: stefano.mocatti@unitn.it; giovanni.marini-2@unitn.it; m.calandrabuonaura@unitn.it

Abstract

Femtosecond pulses have been used to reveal hidden broken symmetry states and induce transitions to metastable states. However, these states are mostly transient and disappear after laser removal. Photoinduced phase transitions towards crystalline metastable states with a change of topological order are rare and difficult to predict and realize experimentally. Here, by using constrained density functional perturbation theory and accounting for light-induced quantum anharmonicity, we show that ultra-fast lasers can permanently transform the topologically-trivial orthorhombic structure of SnSe into the topological crystalline insulating rocksalt phase via a first-order non-thermal phase transition. We describe the reaction path and evaluate the critical fluence and the possible decay channels after photoexcitation. Our simulations of the photoexcited structural and vibrational properties are in excellent agreement with recent pump-probe data in the intermediate fluence regime below the transition with an error on the curvature of the quantum free energy of the photoexcited state that is smaller than 2%.

TOC Graphic



The development of ultrafast laser light with femtosecond (fs) pulses has led to the possibility of inducing a substantial electron-hole population unbalance in semiconductors.¹ After some tens of fs, this electron-hole plasma is well described by a two-chemical potential model, where both electrons and holes are characterized by a thermal distribution. Thus, the ions feel an out-of-equilibrium electronic population with a substantial occupation of conduction or antibonding states that can lead to structural phase transitions before electron-hole recombination takes place. In this scenario, ultrafast pulses can be used to overcome free energy barriers and synthesize crystal structures that cannot be reached by conventional thermodynamical paths. This kind of structural transformation is labeled *non-thermal*, to distinguish it from the much slower ones involved in conventional (*thermal*) material synthesis. Experimental demonstrations of non-thermal phenomena induced by fs pulses are order-disorder phase transitions,² charge density waves,³ non-thermal melting of solids,⁴ transient topological phase transitions⁵ and light-induced suppression of incipient ferroelectricity.⁶ In all these cases, ultrafast light induces short-lived transient states. Much less common are light-induced *non-thermal* permanent structural modifications.

In this work, we show that non-thermal processes can be used to permanently stabilize topological crystalline insulating (TCI) phases.⁷⁻¹¹ In this work, we will focus our attention on tin selenide (SnSe), a IV-VI p-type narrow gap semiconductor that has become popular due to its attracting thermoelectric properties¹²⁻¹⁵ ($zT = 2.6$ at $T = 923$ K). At ambient conditions, tin selenide crystallizes in the orthorhombic $Pnma$ structure, sketched in Fig. 1. At $T \simeq 813$ K¹⁶ or finite pressure,¹⁷ it undergoes a second order phase transition to an orthorhombic $Cmcm$ structure.¹⁷⁻²⁰ In SnSe the topological non-trivial state occurs neither in the $Pnma$ phase, nor in the $Cmcm$ phase, but in a metastable rocksalt structure, which cannot be reached via a thermal transition but it can only be synthesized in thin films via epitaxial growth techniques on a cubic substrate.²¹

Here we design a different approach to obtain the topological crystalline phase of SnSe (see Fig. 1), namely we consider the effect of ultrafast pulses on the topologically trivial $Pnma$

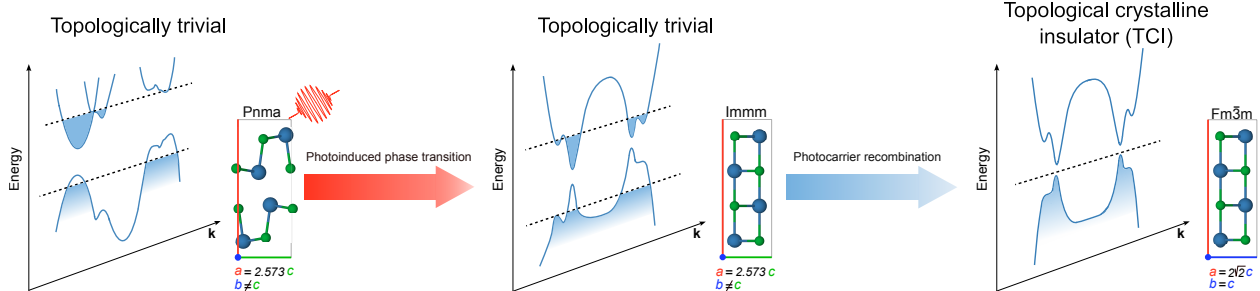


Figure 1: Pictorial representation of the non-thermal pathway connecting the topologically trivial $Pnma$ structure with the TCI $Fm\bar{3}m$ structure. For each phase, sketched crystal structures and band structures are represented. fs pulses induce a first-order transformation toward a transient phase with $Immm$ symmetry. This phase spontaneously decays into the $Fm\bar{3}m$ structure after electron-hole recombination.

phase, which is close to a band inversion.²² By laser pumping with a near-infrared pulse (1.55 eV) and monitoring the time evolution with time-resolved Raman and X-ray diffraction, it was recently shown that structural modifications occur in SnSe, signalled by A_g modes softening and fluence-dependent atomic displacements,²³ interpreted as the precursor of a symmetrization towards a different orthorhombic structure with $Immm$ symmetry. However, no transition to this new crystal phase was detected and first principles simulations were unable to reproduce the observed structural distortion.

In this paper, we investigate the non-thermal structural transformations of the $Pnma$ structure after irradiation with fs pulses by combining constrained density functional perturbation theory (c-DFPT)²⁴ and Stochastic Self-Consistent Harmonic Approximation (SSCHA),²⁵ accounting for quantum anharmonicity in the presence of an electron-hole plasma for the first time. Further technical details are provided in the Supporting Information (SI), which includes Refs. 26–43. We identify the non-thermal pathway (see Fig. 1) and the critical fluence for the structural transition from the ground state $Pnma$ to the transient $Immm$ phase. Our calculated structural distortions and softenings of the A_g modes along the reaction path are in excellent agreement with experimental data.²³ Most importantly, we show that the transient $Immm$ phase spontaneously decays into the TCI rocksalt $Fm\bar{3}m$ SnSe structure after electron-hole recombination and that the structural transformation is

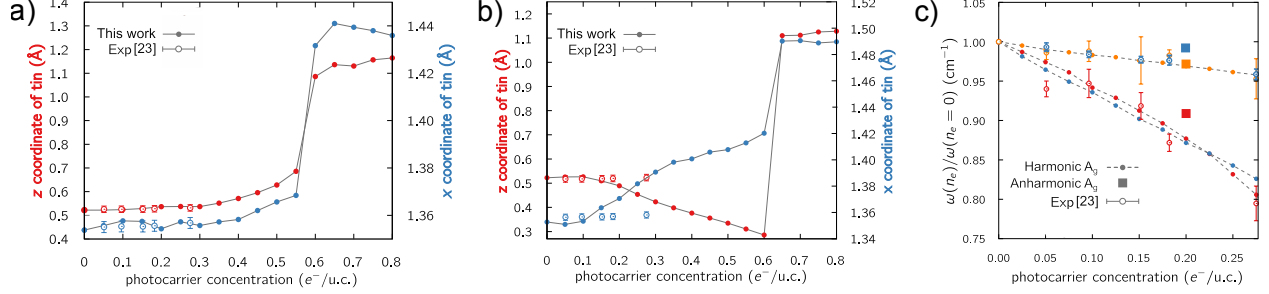


Figure 2: Panels a,b: Tin Wyckoff positions x and z as functions of photocarrier concentration for fixed (a) and variable (b) volume crystal structure optimization. The red and blue dots label the z and x coordinates of tin, respectively. Panel c: Normalized phonon frequencies at Γ for the three relevant A_g modes versus PC. The red, blue and orange dots stand for the $A_{g,1}$, $A_{g,2}$ and $A_{g,4}$ modes, respectively. The theoretical harmonic, anharmonic and experimental values of ω_0 are reported in the SI. The experimental data are from Ref. 23.

permanent in virtue of the free-energy barrier between the rocksalt and the $Pnma$ phase.

In Fig. 2(a),(b) we display the optimized tin Wyckoff x and z coordinates as functions of the photocarrier concentration (PC), n_e , expressed as the number of photoexcited electrons per unit cell (u.c.). Our results are compared with time resolved diffraction data from Ref. 23 (see also SI, Sec.S3) measured in the first 5 ps after illumination. After photoexcitation, both the internal equilibrium positions and the lattice parameters can change. However, the timescale for the two phenomena is generally different.⁴⁴ To unambiguously disentangle cell deformation and internal displacements at fixed cell, we perform structural optimization at fixed cell, Fig. 2(a), and at variable cell, Fig. 2(b) in the presence of an electron-hole plasma (the procedure regarding fluence / PC mapping is reported in the SI).

Our calculation at fixed cell is in excellent agreement with time-resolved X-ray diffraction data in the first 5 ps, while that at variable cell substantially deviates. This confirms that in the first ps after irradiation the atoms are displaced at fixed cell. Previous calculations from Ref. 23, see Fig.S5, obtained Sn displacements one order of magnitude larger than the experimental ones. Conversely, we report an excellent agreement between our c-DFT calculations and experimental data within our framework.²⁴ The stark disagreement among the calculation of Ref. 23 and experiments arises because in Ref. 23 the electron and hole

occupations are not self-consistently relaxed. This procedure does not lead to a correctly thermalized quasi-equilibrium Fermi-Dirac distribution. An explanation of the main differences between the approach of Ref. 23 and the c-DFT approach of Refs. 45 and 24 used in this work is reported in Sec.S3.1 in the SI.

The discontinuity in the z_{Sn} and x_{Sn} in Figs. 2(a),(b) at $n_e^c \approx 0.6 e^-/\text{u.c.}$ signals the occurrence of a first-order phase transition. The phase transition can be easily identified by noting that for $n_e \geq 0.6 e^-/\text{u.c.}$ the Wyckoff positions of tin correspond to that of the *Immm* structure, where they are fixed by symmetry. Thus, we predict the phase transition from *Pnma* to *Immm* to occur at a value of n_e that is approximately a factor of two larger than the highest photocarrier concentration measured in Ref. 23.

Additional validation of our findings arises from the A_g harmonic and anharmonic phonon frequencies calculation at fixed cell. The results are shown in Fig. 2(c) where they are compared with the measured frequencies of oscillation of the Bragg peaks in the first ps after pumping as a function of n_e .²³ We plot the value of the harmonic A_g phonon frequencies (full circles) at a given photocarrier concentration (i.e. $\omega(n_e)$) divided by the harmonic phonon frequency in the ground state (i.e. $\omega_0 = \omega(n_e = 0)$). The softening of the harmonic modes $A_{g,1}$ and $A_{g,4}$ induced by the photoexcitation is in excellent agreement with experimental data. Concerning the $A_{g,2}$ mode, c-DFPT overestimates the softening induced by the electron-hole plasma within the harmonic approximation. A possible reason for this discrepancy is the presence of a strong anharmonic renormalization for the $A_{g,2}$ mode. Thus, we calculated the anharmonic phonon frequencies in the absence of photocarriers and for $n_e = 0.2 e^-/\text{u.c.}$ at $T = 0$ K. Our results are depicted in Fig. 2(c), where the values of the normalized anharmonic phonon frequencies ($\omega(n_e)/\omega_0$) are represented as filled squares. The anharmonic corrections to the phonon frequencies of the $A_{g,1}$ and $A_{g,4}$ modes are mild and do not change the overall trend obtained at the harmonic level. On the contrary, the $A_{g,2}$ mode is substantially affected by anharmonicity, resulting in an improved agreement with the experimental data. The maximum relative error on the predicted quantum phonon

frequency softening is roughly 2%.

The $A_{g,2}$ mode plays a crucial role in the $Pnma \rightarrow Immm$ phase transition. The observed strong anharmonic renormalization of the $A_{g,2}$ mode indicates that the Born-Oppenheimer free energy surface surrounding the minimum energy state corresponding to the $Pnma$ phase is becoming progressively more anharmonic along the path of the transition.

The crucial role of quantum anharmonicity becomes even more evident if the electronic structures together with the harmonic and quantum anharmonic dispersions of the $Pnma$ and $Immm$ phase are considered, in Fig. 3). The insulating ground state (Fig. 3(a)) displays a finite electronic gap (≈ 0.52 eV), and dynamically stable harmonic phonons (Fig. 3(c)). The quantum anharmonic corrections on the phonon spectrum are essentially negligible. On the contrary, the light-induced $Immm$ phase in the presence of an electron-hole plasma at $n_e = 0.6$ $e^-/\text{u.c.}$ has a metallic electronic structure with electron and hole Fermi surfaces located close to the high-symmetry Y and Z points, (Fig. 3(b)). These Fermi surfaces are nested (see SI, Sec. S3) and trigger the emergence of a Peierls instability at the harmonic level signalled by imaginary phonons along the $\Gamma - X$ direction at a wave-vector compatible with the nesting condition (Fig. 3(d)). Structural minimization shows the emergence of a $2 \times 1 \times 1$ one-dimensional chain-like charge density wave with an energy gain of ≈ 1.5 meV/atom with respect to the undistorted structure (see SI). When quantum-anharmonic corrections are included within the SSCHA at $n_e = 0.6$ $e^-/\text{u.c.}$, we find that the instability is removed and a sharp one-dimensional Kohn-anomaly appears (Fig. 3(d)). Thus, light-induced quantum anharmonicity stabilizes the $Immm$ phase in the transient state at $n_e = 0.6$ $e^-/\text{u.c.}$.

The critical PC of $n_e = 0.6$ $e^-/\text{u.c.}$, corresponding to ≈ 4.8 mJ/cm², is achievable in ultrafast experiments similar or larger values have already been achieved in narrow gap semiconductors without inducing significant damage to the sample.⁴⁶⁻⁴⁸

Having demonstrated the accuracy of our approach to describe the structural evolution after photoexcitation, we now try to understand more in detail the reaction path and the nature of this transition. In Fig. 4, we display the energy along the paths relative to the

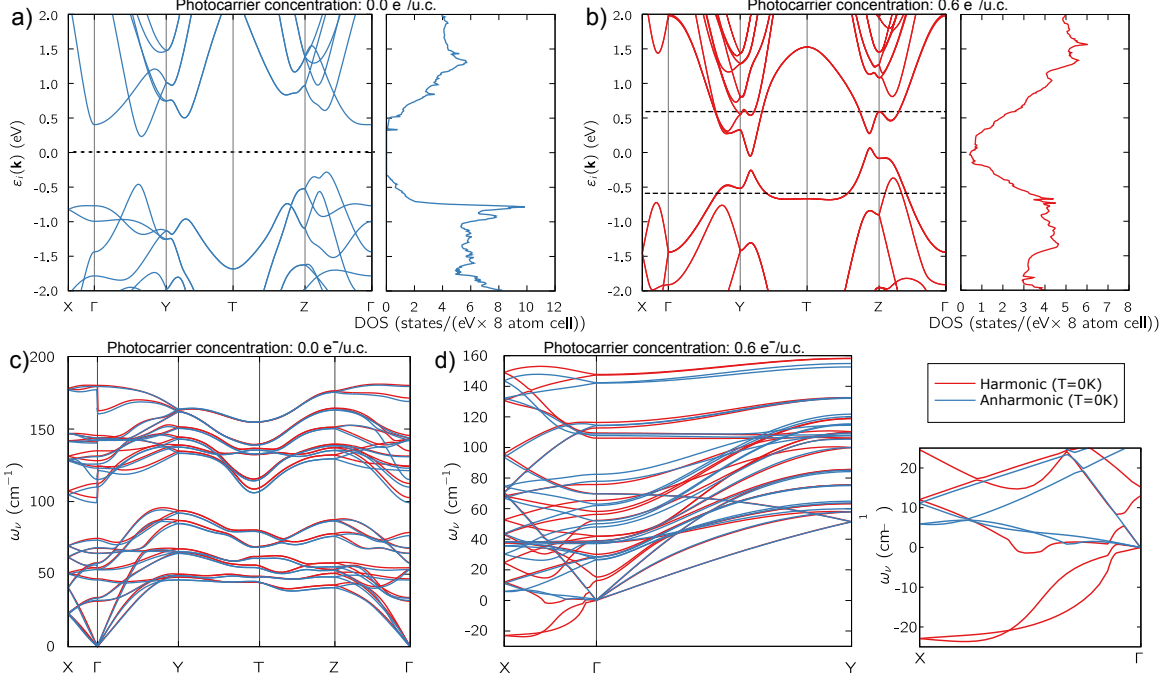


Figure 3: Panels a,b: Ground state electronic structure of the $Pnma$ phase (a) and of the $Immm$ transient phase at $n_e = 0.6 e^-/u.c.$ (b). The Fermi level in (a) and the holes and electrons Fermi levels in (b) are depicted as dashed lines. Panels c,d: harmonic and anharmonic phonon spectra for the $Pnma$ phase at $n_e = 0.0 e^-/u.c.$ (c) and for the transient $Immm$ phase at $n_e = 0.6 e^-/u.c.$ (d). Both plots are at $T = 0$ K. The inset shows the removal of the dynamical instability by quantum anharmonic effects.

(a) $Pnma \rightarrow Immm$ and (b) $Pnma \rightarrow Cmcm$ transitions, for a few values of n_e . The path is parametrized by the reaction coordinate η , where $\eta = 0$ stands for the $Pnma$ structure while $\eta = 1$ represents either the $Immm$ or $Cmcm$ structure.

Considering the $n_e = 0.0 e^-/u.c.$ case, both the reactions toward the $Immm$ and $Cmcm$ present a large kinetic barrier. As the PC is increased, the $Pnma \rightarrow Immm$ barrier is gradually suppressed and becomes zero for $n_e \simeq n_e^c$. Since the lowest energy configuration corresponds to the $Immm$ phase for $n_e > n_e^c$, the $Pnma \rightarrow Immm$ reaction becomes spontaneous. Conversely, the $Pnma \rightarrow Cmcm$ barrier remains finite for every value of PC.

The question arises if the structural transformation towards the $Immm$ is permanent, i.e. if the $Immm$ phase remains stable at longer times after carrier recombination has taken place. To correctly describe the slow structural dynamics, one must also include volume relaxation effects.

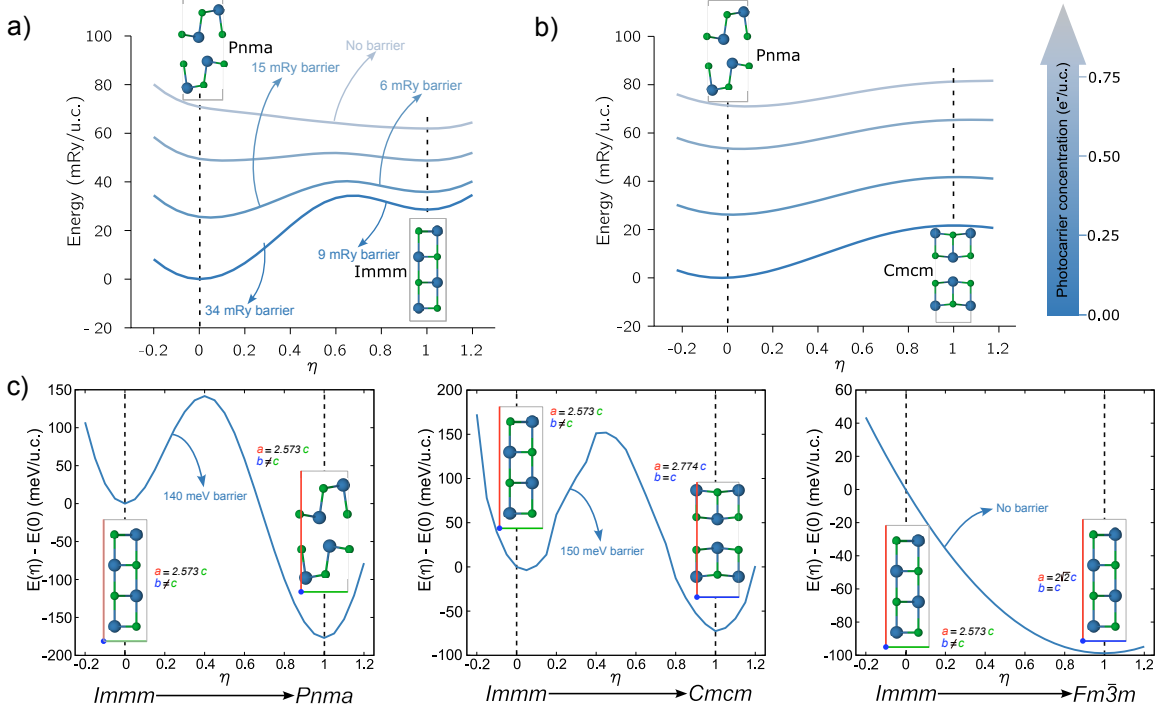


Figure 4: Panels a,b: Total energy curves along the $Pnma \rightarrow Immm$ (a) and $Pnma \rightarrow Cmcm$ (b) reaction paths: $\eta = 0$ corresponds to the $Pnma$ phase while $\eta = 1$ to the $Immm$ (a) or $Cmcm$ (b) phase. Panel c: possible decay channels for the $Immm$ phase: $Immm \rightarrow Pnma$, $Immm \rightarrow Cmcm$ and $Immm \rightarrow Fm\bar{3}m$. We recall that 1 mRy/u.c. corresponds to 40 K while 1 meV/u.c. corresponds to 3 K.

To this aim, we consider variable-volume reaction paths in the absence of photoexcitation starting from the $Immm$ structure, namely $Immm \rightarrow Pnma$, $Immm \rightarrow Cmcm$ and $Immm \rightarrow Fm\bar{3}m$. The initial $Immm$ structure corresponds to the photo-induced transient phase while the final structures are obtained through variable volume optimization with zero PC. Along the reactions, both the internal coordinates and the structural parameters vary. The results of our calculations are shown in Fig. 4(c). Both the transformations $Immm \rightarrow Pnma$ and $Immm \rightarrow Cmcm$ present large energy barriers, thus are not spontaneous. Conversely, the $Immm \rightarrow Fm\bar{3}m$ reaction does not have a barrier and can occur spontaneously. Hence, once the transient $Immm$ phase has been stabilized, electron-hole recombination takes place and the system decays into the TCI $Fm\bar{3}m$ phase.

In addition, we stress that a large free energy barrier, amounting to 15 mRy/u.c., exists between the $Fm\bar{3}m$ and the $Pnma$ (see Fig. S6). Hence, the topological rocksalt phase can

survive thermal fluctuations corresponding to ≈ 600 K before decaying into the *Pnma* phase. This finding demonstrates the occurrence of a non-thermal path stabilizing the SnSe rocksalt structure and provides a non-thermal synthesis mechanism for the rocksalt TCI phase.

We stress the fundamental role played by light-induced symmetrization. The TCI phase of rocksalt-SnSe is protected by a combination of time-reversal and C_4 symmetry, the latter being absent both in the *Pnma* and *Immm* phases. Crucially, we showed that laser irradiation favors the *Pnma* \rightarrow *Immm* symmetrization, allowing the crystal to access a metastable region of the phase diagram, in close proximity to the $Fm\bar{3}m$ structure, which is successively stabilized after the laser removal, finally restoring the cubic C_4 symmetry necessary to protect the topological crystalline order.⁷

In conclusion, we have shown that ultrafast pulses can permanently transform the topologically-trivial *Pnma* phase of SnSe into the TCI rocksalt phase. The mechanism is non-thermal and does not require epitaxial growth on particular substrates. This is one of the rare cases when ultrafast pulses change the topological properties of the material. We identified the transition path and evaluated its critical fluence. A strong validation for the accuracy and predictivity of our theoretical framework is the excellent agreement of our quantum anharmonic calculations in the photoexcited regime with recent pump-probe X-ray free electron-laser measurements in the low fluence regime below the transition.

Finally, we would like to point out that our findings demonstrate that light can be used to reshape the free-energy landscape allowing to access otherwise unreachable regions of the phase diagram. This general result is relevant for the exploration of new phases in a broad class of materials, including monochalcogenides,⁴⁹ highly relevant for energy applications, insulating/semiconducting 2D materials with strong spin-orbit coupling and, in general, all semiconducting materials in the proximity of structural instability.

Funded by the European Union (ERC, DELIGHT, 101052708). Views and opinions expressed are however those of the authors only and do not necessarily reflect those of the European Union or the European Research Council. Neither the European Union nor the

granting authority can be held responsible for them. We acknowledge the CINECA award under the ISCRA initiative, for the availability of high-performance computing resources and support. We acknowledge PRACE for awarding us access to Joliot-Curie at GENCI@CEA, France (project file number 2021240020).

Supporting Information Available

Description of the computational methods, crystal structures and comparison of the two different cDFT approaches.

References

- (1) Maiuri, M.; Garavelli, M.; Cerullo, G. Ultrafast Spectroscopy: State of the Art and Open Challenges. *Journal of the American Chemical Society* **2020**, *142*, 3–15, PMID: 31800225.
- (2) Wall, S.; Yang, S.; Vidas, L.; Chollet, M.; Glowina, J. M.; Kozina, M.; Katayama, T.; Henighan, T.; Jiang, M.; Miller, T. A. et al. Ultrafast disordering of vanadium dimers in photoexcited VO₂. *Science* **2018**, *362*, 572–576.
- (3) Kogar, A.; Zong, A.; Dolgirev, P. E.; Shen, X.; Straquadine, J.; Bie, Y.-Q.; Wang, X.; Rohwer, T.; Tung, I.-C.; Yang, Y. et al. Light-induced charge density wave in late3. *Nature Physics* **2019**, *16*, 159–163.
- (4) Sokolowski-Tinten, K.; Bialkowski, J.; von der Linde, D. Ultrafast laser-induced order-disorder transitions in semiconductors. *Phys. Rev. B* **1995**, *51*, 14186–14198.
- (5) Sie, E. J.; Nyby, C. M.; Pemmaraju, C. D.; Park, S. J.; Shen, X.; Yang, J.; Hoffmann, M. C.; Ofori-Okai, B. K.; Li, R.; Reid, A. H. et al. An ultrafast symmetry switch in a Weyl semimetal. *Nature* **2019**, *565*, 61–66.

- (6) Jiang, M. P.; Trigo, M.; Savić, I.; Fahy, S.; Murray, E. D.; Bray, C.; Clark, J.; Henighan, T.; Kozina, M.; Chollet, M. et al. The origin of incipient ferroelectricity in lead Telluride. *Nature Communications* **2016**, *7*.
- (7) Fu, L. Topological Crystalline Insulators. *Phys. Rev. Lett.* **2011**, *106*, 106802.
- (8) Hsieh, T. H.; Lin, H.; Liu, J.; Duan, W.; Bansil, A.; Fu, L. Topological crystalline insulators in the sntc material class. *Nature Communications* **2012**, *3*.
- (9) Sun, Y.; Zhong, Z.; Shirakawa, T.; Franchini, C.; Li, D.; Li, Y.; Yunoki, S.; Chen, X.-Q. Rocksalt SnS and SnSe: Native topological crystalline insulators. *Phys. Rev. B* **2013**, *88*, 235122.
- (10) Dziawa, P.; Kowalski, B. J.; Dybko, K.; Buczko, R.; Szczerbakow, A.; Szot, M.; Łusakowska, E.; Balasubramanian, T.; Wojek, B. M.; Berntsen, M. H. et al. Topological crystalline insulator states in $\text{Pb}_{1-x}\text{Sn}_x\text{Se}$. *Nature Materials* **2012**, *11*, 1023–1027.
- (11) Ma, J.; Yi, C.; Lv, B.; Wang, Z.; Nie, S.; Wang, L.; Kong, L.; Huang, Y.; Richard, P.; Zhang, P. et al. Experimental evidence of hourglass fermion in the candidate nonsymmorphic topological insulator KHgSb . *Science Advances* **2017**, *3*, e1602415.
- (12) Guo, R.; Wang, X.; Kuang, Y.; Huang, B. First-principles study of anisotropic thermoelectric transport properties of IV-VI semiconductor compounds SnSe and SnS. *Phys. Rev. B* **2015**, *92*, 115202.
- (13) Xie, L.; He, D.; He, J. SnSe, the rising star thermoelectric material: A new paradigm in atomic blocks, building intriguing physical properties. *Materials Horizons* **2021**, *8*, 1847–1865.
- (14) Chandra, S.; Dutta, P.; Biswas, K. High-Performance Thermoelectrics Based on Solution-Grown SnSe Nanostructures. *ACS Nano* **2022**, *16*, 7–14, PMID: 34919391.

- (15) Zhao, L.-D.; Lo, S.-H.; Zhang, Y.; Sun, H.; Tan, G.; Uher, C.; Wolverton, C.; Dravid, V. P.; Kanatzidis, M. G. Ultralow thermal conductivity and high thermoelectric figure of merit in sncs crystals. *Nature* **2014**, *508*, 373–377.
- (16) Chattopadhyay, T.; Pannetier, J.; Von Schnering, H. Neutron diffraction study of the structural phase transition in SnS and SnSe. *Journal of Physics and Chemistry of Solids* **1986**, *47*, 879–885.
- (17) Loa, I.; Husband, R. J.; Downie, R. A.; Popuri, S. R.; Bos, J.-W. G. Structural changes in thermoelectric SnSe at high pressures. *Journal of Physics: Condensed Matter* **2015**, *27*, 072202.
- (18) Ghosh, A.; Gusmão, M.; Chaudhuri, P.; Michielon de Souza, S.; Mota, C.; Trichês, D.; Frota, H. Electrical properties of SnSe under high-pressure. *Computational Condensed Matter* **2016**, *9*, 77–81.
- (19) Adouby, K.; Perez-Vicente, C.; Jumas, J. C. Structure and temperature transformation of SnSe. Stabilization of a new cubic phase Sn₄Bi₂Se₇. *Zeitschrift für Kristallographie - Crystalline Materials* **1998**, *213*, 343–349.
- (20) Aseginolaza, U.; Bianco, R.; Monacelli, L.; Paulatto, L.; Calandra, M.; Mauri, F.; Bergara, A.; Errea, I. Phonon Collapse and Second-Order Phase Transition in Thermoelectric SnSe. *Phys. Rev. Lett.* **2019**, *122*, 075901.
- (21) Mariano, A. N.; Chopra, K. L. POLYMORPHISM IN SOME IV-VI COMPOUNDS INDUCED BY HIGH PRESSURE AND THIN-FILM EPITAXIAL GROWTH. *Applied Physics Letters* **1967**, *10*, 282–284.
- (22) Hong, J.; Delaire, O. Phase transition and anharmonicity in SnSe. *Materials Today Physics* **2019**, *10*, 100093.

- (23) Huang, Y.; Yang, S.; Teitelbaum, S.; De la Peña, G.; Sato, T.; Chollet, M.; Zhu, D.; Niedziela, J. L.; Bansal, D.; May, A. F. et al. Observation of a Novel Lattice Instability in Ultrafast Photoexcited SnSe. *Phys. Rev. X* **2022**, *12*, 011029.
- (24) Marini, G.; Calandra, M. Lattice dynamics of photoexcited insulators from constrained density-functional perturbation theory. *Phys. Rev. B* **2021**, *104*, 144103.
- (25) Monacelli, L.; Bianco, R.; Cherubini, M.; Calandra, M.; Errea, I.; Mauri, F. The stochastic self-consistent harmonic approximation: calculating vibrational properties of materials with full quantum and anharmonic effects. *Journal of Physics: Condensed Matter* **2021**, *33*, 363001.
- (26) Giannozzi, P.; Baroni, S.; Bonini, N.; Calandra, M.; Car, R.; Cavazzoni, C.; Ceresoli, D.; Chiarotti, G. L.; Cococcioni, M.; Dabo, I. et al. QUANTUM ESPRESSO: a modular and open-source software project for quantum simulations of materials. *Journal of Physics: Condensed Matter* **2009**, *21*, 395502.
- (27) Giannozzi, P.; Andreussi, O.; Brumme, T.; Bunau, O.; Nardelli, M. B.; Calandra, M.; Car, R.; Cavazzoni, C.; Ceresoli, D.; Cococcioni, M. et al. Advanced capabilities for materials modelling with Quantum ESPRESSO. *Journal of Physics: Condensed Matter* **2017**, *29*, 465901.
- (28) Hamann, D. R. Optimized norm-conserving Vanderbilt pseudopotentials. *Phys. Rev. B* **2013**, *88*, 085117.
- (29) Perdew, J. P.; Burke, K.; Ernzerhof, M. Generalized Gradient Approximation Made Simple. *Phys. Rev. Lett.* **1996**, *77*, 3865–3868.
- (30) Grimme, S.; Antony, J.; Ehrlich, S.; Krieg, H. A consistent and accurate ab initio parametrization of density functional dispersion correction (DFT-D) for the 94 elements H-Pu. *The Journal of Chemical Physics* **2010**, *132*, 154104.

- (31) Monkhorst, H. J.; Pack, J. D. Special points for Brillouin-zone integrations. *Phys. Rev. B* **1976**, *13*, 5188–5192.
- (32) Sundaram, S. K.; Mazur, E. Inducing and probing non-thermal transitions in semiconductors using femtosecond laser pulses. *Nature Materials* **2002**, *1*, 217–224.
- (33) Marzari, N.; Vanderbilt, D.; De Vita, A.; Payne, M. C. Thermal Contraction and Disorder of the Al(110) Surface. *Phys. Rev. Lett.* **1999**, *82*, 3296–3299.
- (34) Baroni, S.; de Gironcoli, S.; Dal Corso, A.; Giannozzi, P. Phonons and related crystal properties from density-functional perturbation theory. *Rev. Mod. Phys.* **2001**, *73*, 515–562.
- (35) Kokalj, A. Computer graphics and graphical user interfaces as tools in simulations of matter at the atomic scale. *Computational Materials Science* **2003**, *28*, 155–168, Proceedings of the Symposium on Software Development for Process and Materials Design.
- (36) Momma, K.; Izumi, F. *VESTA3* for three-dimensional visualization of crystal, volumetric and morphology data. *Journal of Applied Crystallography* **2011**, *44*, 1272–1276.
- (37) Bansal, D.; Hong, J.; Li, C. W.; May, A. F.; Porter, W.; Hu, M. Y.; Abernathy, D. L.; Delaire, O. Phonon anharmonicity and negative thermal expansion in SnSe. *Phys. Rev. B* **2016**, *94*, 054307.
- (38) Li, C. W.; Hong, J.; May, A. F.; Bansal, D.; Chi, S.; Hong, T.; Ehlers, G.; Delaire, O. Orbitally driven giant phonon anharmonicity in SnSe. *Nature Physics* **2015**, *11*, 1063–1069.
- (39) Gong, X.; Wu, H.; Yang, D.; Zhang, B.; Peng, K.; Zou, H.; Guo, L.; Lu, X.; Chai, Y.; Wang, G. et al. Temperature dependence of Raman scattering in single crystal SnSe. *Vibrational Spectroscopy* **2020**, *107*, 103034.

- (40) Shi, G.; Kioupakis, E. Quasiparticle band structures and thermoelectric transport properties of p-type SnSe. *Journal of Applied Physics* **2015**, *117*, 065103.
- (41) Blöchl, P. E.; Jepsen, O.; Andersen, O. K. Improved tetrahedron method for Brillouin-zone integrations. *Phys. Rev. B* **1994**, *49*, 16223–16233.
- (42) Nikolić, P. M.; Milković, L.; Mihajlović, P.; Lavrenčić, B. Raman scattering in snse. *Czechoslovak Journal of Physics* **1978**, *28*, 456–459.
- (43) Huang, Y.; Teitelbaum, S.; Yang, S.; na, G. D. I. P.; Chollet, T. S. M.; Zhu, D.; Niedziela, J. L.; Bansal, D.; May, A. F.; Lindenberg, A. M. et al. Determination of nonthermal bonding origin of a novel photoexcited lattice instability in SnSe. 2023; <https://arxiv.org/abs/2301.08955>.
- (44) Reis, D. A.; Lindenberg, A. M. Ultrafast X-ray scattering in solids. *Topics in Applied Physics* **2006**, 371–422.
- (45) Tangney, P.; Fahy, S. Density-functional theory approach to ultrafast laser excitation of semiconductors: Application to the A_1 phonon in tellurium. *Phys. Rev. B* **2002**, *65*, 054302.
- (46) Hu, J.; Vanacore, G. M.; Yang, Z.; Miao, X.; Zewail, A. H. Transient Structures and Possible Limits of Data Recording in Phase-Change Materials. *ACS Nano* **2015**, *9*, 6728–6737, PMID: 26035229.
- (47) Cavalleri, A.; Tóth, C.; Siders, C. W.; Squier, J. A.; Ráksi, F.; Forget, P.; Kieffer, J. C. Femtosecond Structural Dynamics in VO₂ during an Ultrafast Solid-Solid Phase Transition. *Phys. Rev. Lett.* **2001**, *87*, 237401.
- (48) Wall, S.; Yang, S.; Vidas, L.; Chollet, M.; Glowonia, J. M.; Kozina, M.; Katayama, T.; Henighan, T.; Jiang, M.; Miller, T. A. et al. Ultrafast disordering of vanadium dimers in photoexcited VO₂. *Science* **2018**, *362*, 572–576.

(49) Behnia, K. Finding merit in dividing neighbors. *Science* **2016**, *351*, 124–124.